# Nanostructured Metallo-Dielectric Quasi-Crystals: Towards Photonic-Plasmonic Resonance Engineering

*Alessio Crescitelli, Armando Ricciardi, Marco Consales, Emanuela Esposito,* Carmine Granata, Vincenzo Galdi, Antonello Cutolo, and Andrea Cusano**

**The first evidence of out-of-plane resonances in hybrid metallo-dielectric quasi-crystal (QC) nanostructures composed of metal-backed aperiodically patterned low-contrast dielectric layers is reported. Via experimental measurements and full-wave numerical simulations, these resonant phenomena are characterized with specific reference to the Ammann-Beenker (quasi-periodic, octagonal) tiling lattice geometry and the underlying physics is investigated. In particular, it is shown that, by comparison with standard periodic structures, a moderately richer spectrum of resonant modes may be excited, due to the easier achievement of phase-matching conditions endowed by its denser Bragg spectrum. Such modes are characterized by a distinctive plasmonic or photonic behavior, discriminated by their field distribution and dependence on the metal film thickness. Moreover, the response is accurately predicted via computationally affordable periodic-approximant-based numerical modeling. The enhanced capability of QCs to control number, spectral position, and mode distribution of hybrid resonances may be exploited in a variety of possible applications. To assess this aspect, label-free biosensing is studied via characterization of the surface sensitivity of the proposed structures with respect to local refractive index changes. Moreover, it is also shown that the resonance-engineering capabilities of QC nanostructures may be effectively exploited in order to enhance the absorption efficiency of thin-film solar cells.**

## 1. Introduction

Currently, there is a great deal of interest in the study of out-of-plane resonances occurring in nanostructured metallic and dielectric films, stimulated by the formidable advances in nanofabrication technologies and the possible disruptive applications to highly strategic fields such as chemical and biological sensing as well as nonlinear optics and thin-film solar cells. It is well known that flat metallic films can support surface plasmon polaritons (SPPs), which are due to coherent oscillations of the surface charge density bound at the metal surface,[1,2] and may be excited through prism- or grating-based coupling schemes. Moreover, nanostructured (e.g., holey, ridged) metallic films may also give rise to local surface plasmon resonances which, in contrast with propagating SPPs, are confined around the nanostructure, and exhibit higher local field intensity.[3] On the other hand, dielectric photonic crystals (PCs),[4] in the simpler 2D form of holey slabs or mono-layers of spheres, can support guided resonances (GRs) due to the coupling of leaky modes with the continuum of radiative modes of the surrounding environment.[5] Both types of resonant phenomena (henceforth, simply referred to as "plasmonic" and "photonic," respectively) are characterized by peculiar spectral features and selectivity.

Recent studies[6–12] have demonstrated the very promising potentials of hybrid platforms based on metallo-dielectric nanostructures capable of supporting both plasmonic and photonic resonances. Following up on the numerical evidence on 1D structures,[6] 2D nanostructured metallo-dielectric plasmonic-photonic crystals have been successfully fabricated[7–12] via self-assembly of a dielectric PC structure constituted by a monolayer of colloidal spheres on a metallic film. Such hybrid structures may exhibit very high-quality-factor (about an order of magnitude larger than typical plasmonic crystals) plasmonic and photonic resonant modes, with a high degree of tunability (e.g., by changing the PC filling-factor and lattice) and a strong sensitivity (with atomic-layer resolution) to external materials deposited on the dielectric PC surface. The inherent richness of interplaying resonant phenomena renders these structures extremely promising candidates for a variety of applications including chemical and biological sensing,[7] tunable light-emitting and active filtering devices,[7–9] as well as solar cells,[13] just to mention a few.

Dr. A. Crescitelli, Dr. A. Ricciardi, Dr. M. Consales, Prof. A. Cutolo, Prof. A. Cusano
Optoelectronic Division
Department of Engineering
University of Sannio
C.so Garibaldi 107, I-82100, Benevento, Italy
E-mail: a.cusano@unisannio.it
Dr. E. Esposito, Dr C. Granata, Prof. A. Cusano
CNR-ICIB "E. Caianiello"
Via Campi Flegrei, 34, I-80078 Pozzuoli (NA), Italy
E-mail: e.esposito@cib.na.cnr.it
Prof. V. Galdi
CNR-SPIN and Waves Group
Department of Engineering
University of Sannio
C.so Garibaldi 107, I-82100, Benevento, Italy

**DOI: 10.1002/adfm.201200217**

The above plasmonic-photonic structures are inherently based on periodic nanostructuring, which can be easily achieved via self-assembly. However, recent studies on either plasmonic (e.g., arrays of sub-wavelength holes in metallic screens,[14,15] and arrays of plasmonic nanoparticles)[16–18] or photonic (holey dielectric slabs)[19] structures, have demonstrated the possible advantages of using aperiodically ordered lattice geometries. Such geometries, inspired by the concept of "quasi-crystal" (QC) in solid-state physics,[20,21] may be effectively modeled by "aperiodic tilings"[22] that are devoid of any translational invariance but can still exhibit long-range order and diffraction spectra characterized by Bragg-like sharp peaks. As a consequence, they retain the essential characteristics of periodic-like light scattering (and, hence, the possibility of exciting plasmonic/photonic resonances) while introducing additional geometric degrees of freedom (e.g., higher-order non-crystallographic rotational symmetries, richer spatial spectra and defect states, etc.) that can be judiciously exploited for tuning/optimizing the response.

In this paper, we present for the first time a numerical and experimental study of hybrid plasmonic and photonic resonances in nanostructured low-contrast metallo-dielectric QCs. Although the discovery of QC colloidal solutions has recently been reported,[23] self-assembly of photonic QCs is not yet a technologically viable option. Therefore, our fabrication procedure is based on standard electron-beam nanolithography. In particular, we design and fabricate a structure composed of a holey dielectric layer, patterned according to the Ammann-Beenker (quasi-periodic, octagonal) tiling, laid on an (unpatterned) aluminum film, and characterize its out-of-plane optical response in terms of plasmonic and photonic resonances. Moreover, to better illustrate the aperiodic-order-induced effects, we compare the results with those pertaining to a standard periodic (square) geometry with same filling factor, highlighting similarities and differences.

## 2. Hybrid Metallo-Dielectric Quasi-Crystal

The hybrid metallo-dielectric nanostructure considered in this study is schematically represented in **Figure 1**a. It essentially consists of a patterned (holey) dielectric layer backed by an unpatterned nanosized metallic (aluminum) film laid on a sapphire substrate. The pattern is based on the octagonal (Ammann-Beenker) quasi-periodic tiling,[22,24] which, as shown in Figure 1b, is composed of square and rhombus tiles whose sidelength $a$ is conventionally assumed to be the characteristic scale (lattice constant). The scanning electron microscopy (SEM) image of the fabricated structure is shown in **Figure 2**a. In order to highlight similarities and differences with the standard (periodic) case, we also fabricated a square-lattice crystal (shown in Figure 2b), with same lattice constant (period, in this case) and slightly different hole radius, in order to equalize the filling factor (≈21%). With the aid of SEM metrology tools, the hole diameter was found to be 480 nm for the QC case (Figure 2a), and 510 nm for the periodic case (Figure 2b), while the lattice constant $a$ was found to be 1 μm in both cases.

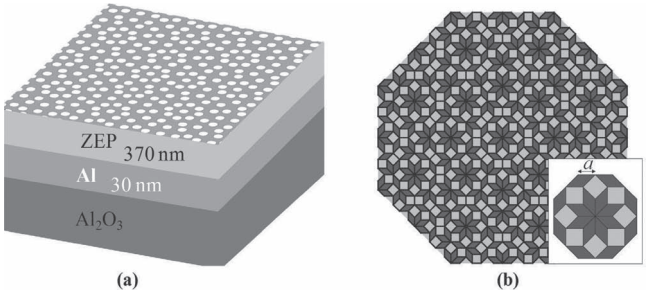


**Figure 1.** a) 3D schematic (not to scale) of the hybrid metallo-dielectric structure with indication of the layer thickness values. b) Ammann-Beenker tiling (third stage) obtained via an iterative (inflation-rule) algorithm,[24] with a zoom of the central region and the lattice constant $a$ (square/rhombus tile sidelength) shown in the inset.

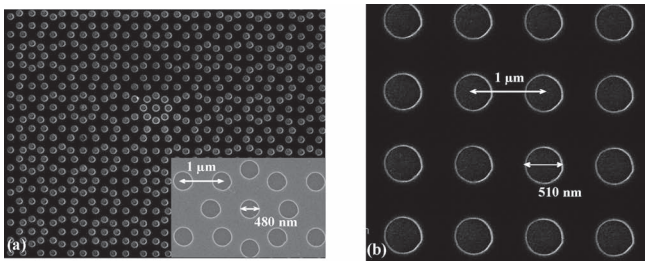


**Figure 2.** SEM images of the QC (a) and square (b) lattices patterned onto the ZEP layer. Holes are placed at the vertices of the tilings. The inset in (a) shows a magnified detail. The measured values of lattice constant $a$ = 1 μm and hole diameter (480 nm in (a), and 510 nm in (b)) are also indicated.

In order to characterize the hybrid photonic-plasmonic resonant behavior of the fabricated samples, we performed out-of-plane spectral reflectance measurements at normal incidence, via a standard reflection setup. The measured reflectance spectra at normal-incidence are shown as solid lines in **Figure 3**a,b for the QC and periodic structures, respectively. For the QC case (Figure 3a), three sharp resonant dips appear at 934 nm (with quality factor $Q \approx 41$), 1146.5 nm ($Q \approx 51$) and 1466 nm ($Q \approx 89$). For the periodic case, two dips are observed at 1100 nm ($Q \approx 74$) and 1367 nm ($Q \approx 84$).

### 2.1. Numerical Simulations

We also carried out numerical studies based on full-wave simulations (via the finite-element-based commercial software package COMSOL Multiphysics,[25] and dispersive, lossy models for the material refractive indexes)[26] aimed at assessing the predictability of the resonant phenomena and understanding their physical nature. For the simpler periodic case, also in view of the mirror symmetries involved, the computational domain was reduced to one-quarter of the unit-cell (shown as an inset in Figure 3b) with perfectly electric-conducting (PEC) and perfectly magnetic-conducting (PMC) in-plane terminations, compatible with normal-incidence illumination. In the more complex QC case, where the use of the unit-cell concept is prevented by the lack of translational symmetry, we relied on a periodic approximant based on a suitably large square "supercell" of sidelength

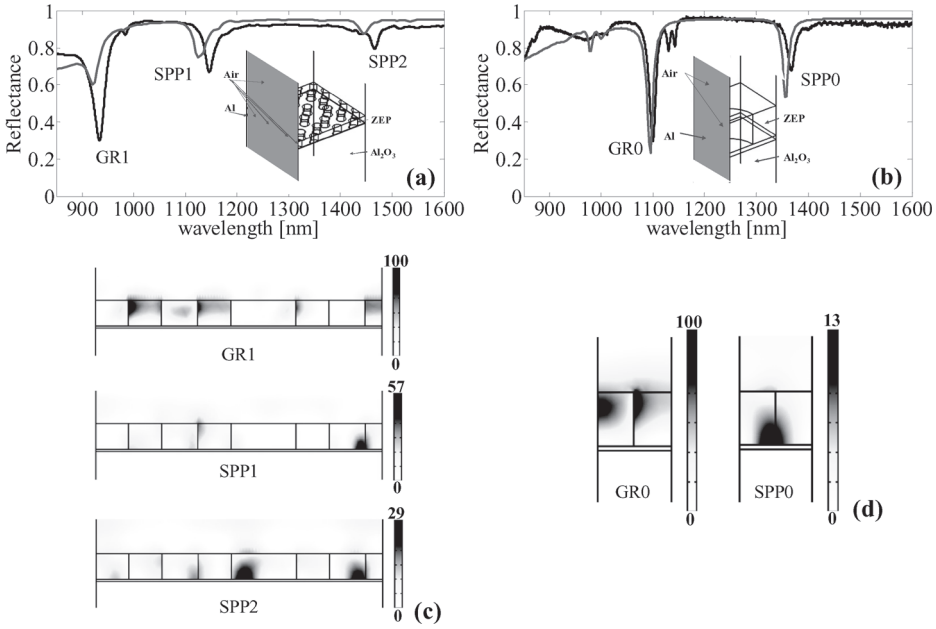


**Figure 3.** a,b) Experimental (solid lines) and numerical (dashed lines) reflectance spectra of the hybrid metallo-dielectric QC and periodic samples shown in Figure 2a,b, respectively. The insets show the (quarter of) supercell (a) and unit-cell (b) used in the simulations. c,d) Electric field intensity maps (normalized with respect to the maximum value observed) at the reflectance minima in a section of the structure (shaded wall in the inset) for the QC and periodic case, respectively.

$L = (4 + 3\sqrt{2})a$. Such a supercell size was chosen as a reasonable tradeoff between model fidelity (i.e., minimization of the possible artifacts introduced by the artificial periodicity) and computational affordability, also on the basis of the outcomes from our previous studies on dielectric QCs.[19] Within this framework, we also exploited the inherent mirror symmetry which allowed the reduction to a single quarter (see the inset in Figure 3a).

The numerically computed reflectance spectra, also shown (as dashed curves) in Figure 3a,b, are in good agreement with the experimental results. The slight discrepancies in the resonant wavelengths and dip amplitudes are attributable to fabrication tolerances in the hole diameters and film thicknesses, whereas the small extra dips experimentally observed (but not predicted numerically) in the periodic case (cf. Figure 3b) are likely due to imperfect (slightly oblique) incidence conditions. Overall, the above results demonstrate the actual applicability and effectiveness of periodic-approximant-based numerical modeling for hybrid QCs, which constitutes an important aspect of our study and provides a viable path for their design for specific applications.

### 2.2. Resonance Classification

As anticipated,[6–12] the resonant dips in Figure 3a,b are attributable to the excitation of plasmonic (SPP) and photonic (GR) modes. In the hybrid structure considered here, the patterned dielectric layer plays a two-fold role, acting both as a diffraction grating for the excitation of SPPs and, at the same time, as a guiding layer supporting photonic GRs.

As it can be observed from Figure 3c, for the QC case, the lowest-wavelength resonance exhibits a field distribution mostly concentrated in the dielectric region, and may accordingly be classified as photonic[5] (henceforth labeled as GR1). Conversely, both the dips at 1146.5 nm and 1466 nm are attributable to plasmonic resonances (SPP1 and SPP2, respectively), since their field distributions turn out to be mostly bound at the metal-film interface.[1] Likewise, for the periodic case shown in Figure 3d, the resonance occurring at 1100 nm can be classified as photonic (GR0), whereas the one located at 1367 nm as plasmonic (SPP0).

As a further validation of the above classification, we fabricated and characterized two additional samples with different values of aluminum thickness $t_{Al}$ (10 nm and 20 nm), with the other geometrical parameters kept constant. As it can be observed from **Figure 4**a,b, far away from the resonant wavelengths, the general effect of decreasing the aluminum film thickness is a shift towards lower values of the reflectance baseline. However, closer to the resonances, two markedly different trends are observed. While the photonic resonances essentially maintain its visibility (consistently with the passive reflective-mirror role played by the metal film), the plasmonic resonances progressively become less sharp and less pronounced (consistently with the active role played by the metal film in supporting SPPs). In particular, for both the QC and periodic cases, the higher-wavelength plasmonic resonances practically disappear for $t_{Al}$ = 10 nm. As a further indication, Figure 4c,d show the corresponding field distributions for the QC and periodic case, respectively. Differently from the photonic case, the plasmonic resonances are excited when $t_{Al}$ approaches 20 nm. Moreover, for increasing aluminum thickness, it can be observed that the resonant field distributions tend to become more concentrated

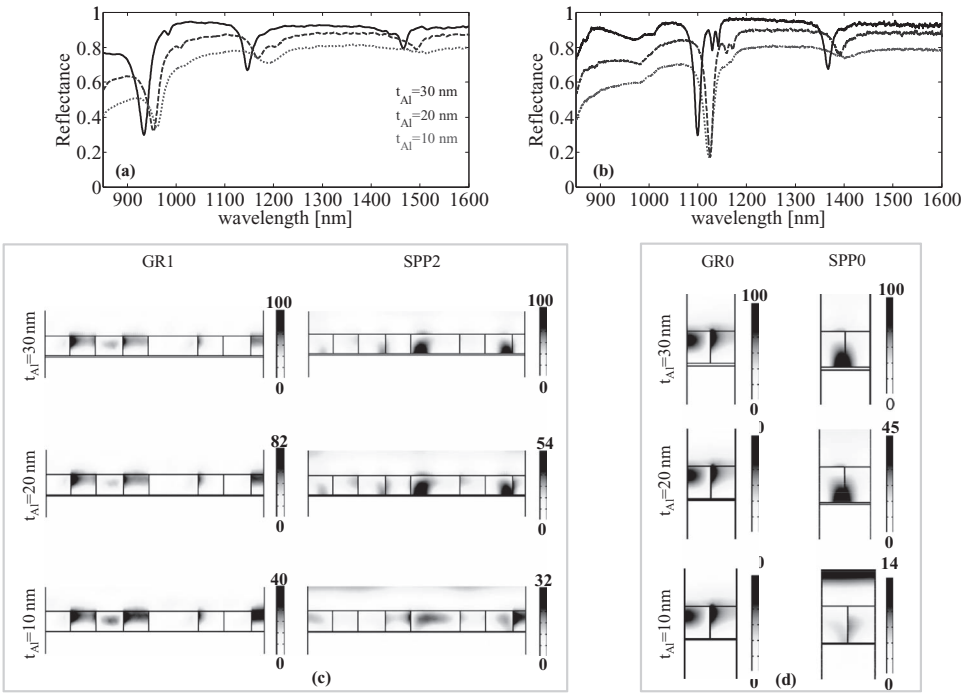


**Figure 4.** a,b) Experimental reflectance of the QC and periodic structures, respectively, for values of the aluminum film thickness $t_{Al}$ = 30, 20, 10 nm (solid lines, dashed lines, dotted lines, respectively). c,d) Electric field intensity for the QC and periodic structures, respectively, at the reflectance minima for photonic (first column) plasmonic (second column), and different values of the aluminum film thickness.

(in the dielectric layer, for the photonic case; at the metal-film interface, for the plasmonic case). This may justify the blue-shift observed in Figure 4a,b, which, consistently with numerical predictions,[27] is much stronger in the plasmonic case. However, small differences in the hole radii among the different samples (due to fabrication tolerances) may also contribute to such blue-shift.

We point out that, although no specific parameter optimization was performed, the *Q*-factors exhibited by our hybrid metallo-dielectric structures are significantly larger than those observed in typical plasmonic crystal configurations.[28–31] To summarize, in our parameter configuration, the highest *Q*-factor was observed for a plasmonic resonance in the QC case. More important, the QC structure was found to exhibit a moderately richer resonant spectrum, with a resonance dip amplitude comparable with the periodic counterpart.

### 2.3. Mode Coupling Mechanism: Towards Resonance Engineering

From the physical viewpoint, the observed resonant phenomena may be understood via approximate semi-analytical models[32] based on phase-matching conditions between Bragg-type peaks in the lattice spatial spectrum (reciprocal lattice) and the photonic and plasmonic bound modes supported by an effective homogenized structure. For instance, **Figure 5**a shows

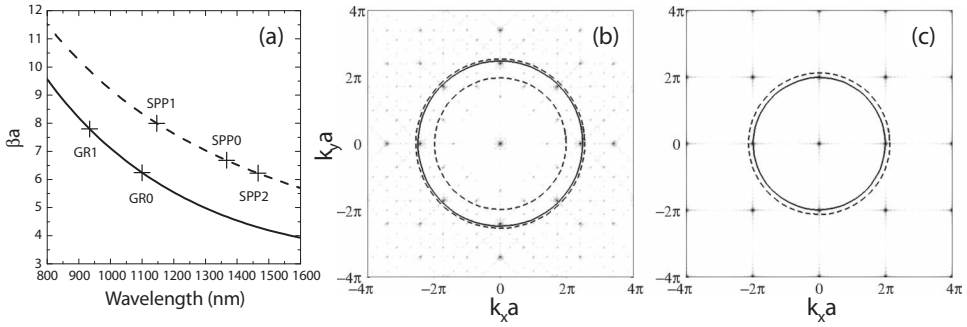


**Figure 5.** a) Dispersion curves of the lowest-order anti-symmetrical TE bound mode supported by a homogenized grounded dielectric slab waveguide (solid line), and the SPP mode supported at the interface between the aluminum and homogenized-dielectric media (dashed line). b,c) Spatial spectra of the QC and periodic PC, respectively, with overlayed the circles of radii $\beta\alpha$ pertaining to the resonant wavelengths (marked with crosses and labeled in the dispersion curves).

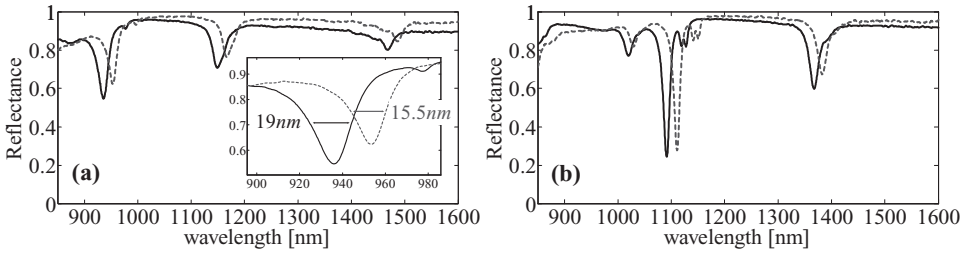


**Figure 6.** a,b) Reflectance spectra for uncoated (solid lines) and 15 nm SiO-coated (dashed lines) QC and periodic structures, respectively. The inset shows a magnified detail around the GR1 dip, with indication of the 3 dB linewidths.

the dispersion curves for i) the lowest-order anti-symmetric transverse-electric ($TE_1$) photonic bound mode supported by a homogenized (assuming a filling factor of 21%) dielectric slab waveguide backed by a perfectly conducting metallic wall[33] (solid line), and ii) the SPP mode supported at the interface between the aluminum and homogenized-dielectric media[1] (dashed line). From these curves, it is possible to extract the in-plane propagation constant (real part, normalized to the lattice constant *a*) pertaining to the resonant wavelengths in Figure 3,4 (marked with crosses and labeled in Figure 5a), and therefore assess the phase-matching conditions $\beta a = |k_n|a$ (with $k_n$ denoting a Bragg wave-vector in the reciprocal space) by drawing circles of radii $\beta\alpha$ overlayed on the spatial spectra of the QC and periodic PC, as shown in Figure 5b,c, respectively. It can be observed that, for both the QC and periodic PC case, all the circles fall rather close to certain orders of spectral peaks, and may therefore be associated to the corresponding phase-matching conditions. As a further illustration of the inherent richness of resonant phenomena in these hybrid structures, it is also observed that the same order of spectral peaks can yield resonances at different wavelengths by interacting with both a photonic and plasmonic mode (e.g., GR1 and SPP1, or GR0 and SPP0).

Moreover, by comparing Figure 5a,b, the inherently denser character of the QC spatial spectrum clearly emerges, with the consequent easier achievement of phase-matching conditions. It is therefore not surprising that the QC structure may exhibit a higher number of resonances and offer extra degrees of freedom for their design.

For a deeper understanding of this aspect, in the Supporting Information we show, with reference to a deterministic aperiodic geometry based on a 1D generalized-Fibonacci sequence,[34] how it is possible to control the Bragg-like peaks in its spatial spectrum (and consequently the phase matching conditions to engineer the resonances) by simply changing a characteristic scale-ratio parameter.

The intrinsic difference of the nature and spacing of the resonances in a QC can be exploited in a number of applications, such as solar cells or nonlinear phase matching, as well as chemical and biological sensing. For instance, in thin-film solar cells, the resonance spacing and coupling strength may be adjusted so as to match the spectral profile of the absorbing layer, whereas in nonlinear phase matching, non-evenly spaced resonances may be useful in order to compensate for material dispersion. An additional feature of these structures is their potential ability to tailor the resonant optical field distribution so as to enhance the spectral sensitivity to local environmental changes, which plays a fundamental role in label-free sensors for chemical and biological detection.

## 3. Study of the Local Refractive Index Sensitivity

We now move on to comparing the performance of hybrid QCs with their periodic counterparts in a variety of strategic fields of application. First, with reference to response tuning/optimization as well as label-free chemical and biological sensing, we focus on the dependence of the hybrid resonances exhibited by the fabricated samples on local refractive index changes, so as to assess their surface sensitivity. Subsequently, in connection with the energy-harvesting field, we also present a comparative study on the application of 1D periodic- and QC-based nanostructures as advanced backreflectors for thin-film solar-cell photovoltaics.

We start considering the effects of nanoscale high-refractive-index (HRI) overlays, which represent an effective approach typically exploited for tailoring the modal distributions and tuning the spectral responses of optical components.[35] We deposited a 15 nm-thick layer of SiO (refractive index ≈ 1.99) on the surface of our fabricated (QC and periodic) samples, by using a thermal evaporation technique at a pressure of $5 \times 10^{-6}$ Torr with a deposition rate of 6.5 Å/s. The reflectance spectra of the SiO-coated and uncoated (QC and periodic) structures are compared in **Figure 6**. As it can be observed, the HRI deposition produces three main effects: i) a red-shift of all resonant modes, ii) the improvement of the quality factor of both photonic and plasmonic resonances, and iii) an increase of the reflectance baseline, also accompanied by a decrease of the resonance visibility. Specifically, for the QC case (Figure 6a), photonic and plasmonic resonances shift towards longer wavelengths (consistent with an increase of the effective refractive index of the resonant modes due to the higher refractive index of the overlay with respect to the patterned dielectric),[35] also exhibiting a dip amplitude deterioration of ≈18%. This clearly reveals that the SiO deposition, as expected, occurs both on the top surface of the structure and inside its holes, thereby enabling the electric field associated to both photonic and plasmonic modes to be modified by the local HRI change when the coating material is applied. In particular, the red-shift exhibited by the plasmonic resonances SPP1 and SPP2 ($\Delta\lambda_{SPP1} = 17.6$ nm and $\Delta\lambda_{SPP2} = 18.0$ nm) is more pronounced than that observed in the photonic case ($\Delta\lambda_{GR1} = 17.2$ nm). A qualitatively similar

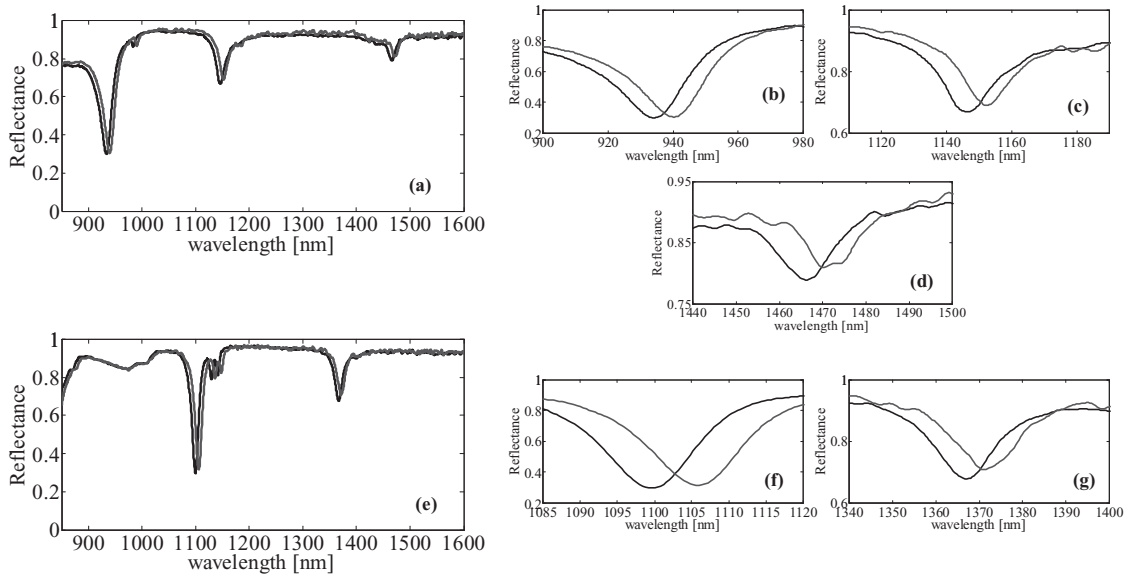


**Figure 7.** a,e) Reflectance spectra for uncoated (solid lines) and 15 nm-$SiO_2$ coated (dashed lines) QC and periodic structures, respectively. Magnified details around the resonance dips are shown in (b–d) and (f,g), respectively.

behavior is obtained in the periodic case (Figure 6b), where red-shifts of the same order are also observed for both the GR0 and SPP0 resonances. Here, however, the shift associated to the photonic resonance ($\Delta\lambda_{GR0}$ = 19.2 nm) turns out to be larger than the plasmonic one ($\Delta\lambda_{SPP0}$ = 15.2 nm).

From the above results, assuming a linear relationship between the wavelength shift and the overlay thickness,[7] a resonance tuning as fine as 1–1.2 nm per nm of HRI overlay may be estimated. This may be an effective device for compensating the few-nanometer fluctuations in the resonant wavelength that may occur from sample to sample due to fabrication tolerances, thereby enabling for a batch-to-batch tuning for the specific application. Moreover, the exploitation of suitable active HRI materials may open up promising perspectives for actively (e.g., electronically, magnetically, thermally) tuning the resonances.

Another important advantage of the HRI deposition is the *Q*-factor enhancement, as clearly observable from Figure 6. In particular, with reference to the QC case in Figure 6a, a 27% *Q*-factor enhancement was calculated for the photonic resonance GR1 (see the inset for a magnified detail around the dip), as well as of nearly 12% and 8% for the plasmonic resonances SPP1 and SPP2, respectively. This effect is also observed for the periodic structure, but with a weaker *Q*-factor enhancement, namely ≈9% for the photonic resonance GR0, and no sensible variation for the plasmonic resonance SPP0.

In order to explore possible applications to chemical and biological sensing, we also carried out (via radio-frequency sputtering at an Ar pressure of 3mTorr with a rate of 3.7 Å/s) the deposition of nanoscale (15 nm thick) overlays of $SiO_2$ (refractive index ≈ 1.45), which well resembles the binding typical of biomolecular interactions.[36,37]

**Figure 7**a compares the reflectance spectra of the QC structure before and after the deposition. Also in this case, a red-shift of both resonance types occurs, but less evident than the SiO case, mainly due to the lower refractive index of $SiO_2$. In particular, the photonic resonance GR1 exhibits a slightly larger shift ($\Delta\lambda_{GR1}$ = 6.4 nm) than the plasmonic ones SPP1 and SPP2 ($\Delta\lambda_{SPP1} = \Delta\lambda_{SPP2}$ = 6.0 nm). For comparison, we show in Figure 7e the reflectance spectra of the uncoated and $SiO_2$-coated periodic samples. Also in this case, the wavelength shift observed for the photonic resonance GR0 ($\Delta\lambda_{GR0}$ = 6.4 nm) is slightly larger that that associated to the plasmonic one SPP0 ($\Delta\lambda_{SPP0}$ = 4.0 nm). Overall, the plasmonic resonances in the QC case turn out to exhibit higher sensitivity than their periodic counterpart, with enhancement up to 50%.

The above results reveal promising molecular sensitivity at monolayer scale, namely, surface sensitivities (in terms of resonance shift per nanometer of deposited overlay) as high as 0.40 nm and 0.43 nm for the plasmonic and photonic resonances, respectively. Considering the typical sizes of biological molecules (3.8–5.2 nm), it can be inferred that the binding of a single biological monolayer to the sample surface is able to generate a resonance shift of approximately 1.5–2 nm, which may be easily detected via a low-cost commercial spectrophotometer.

Moreover, for the QC case, the actual tiling geometry constitutes an important degree of freedom for tailoring the field distribution of the resonant modes, and thus there exist further margins of improvement for the surface sensitivity. For instance, in a recent numerical parametric study on dielectric free-standing structures[38] we showed that, for a given parameter configuration (slab thickness and refractive index, and filling factor), sensitivity enhancements up to a factor of seven could be achieved solely by changing the hole spatial arrangement from periodic (square) to aperiodic (octagonal).

We point out that the obtained sensitivity performance cannot be directly compared with single/few-molecule detection schemes.[39–43] Indeed, these configurations are often characterized by comparable surface sensitivities but very

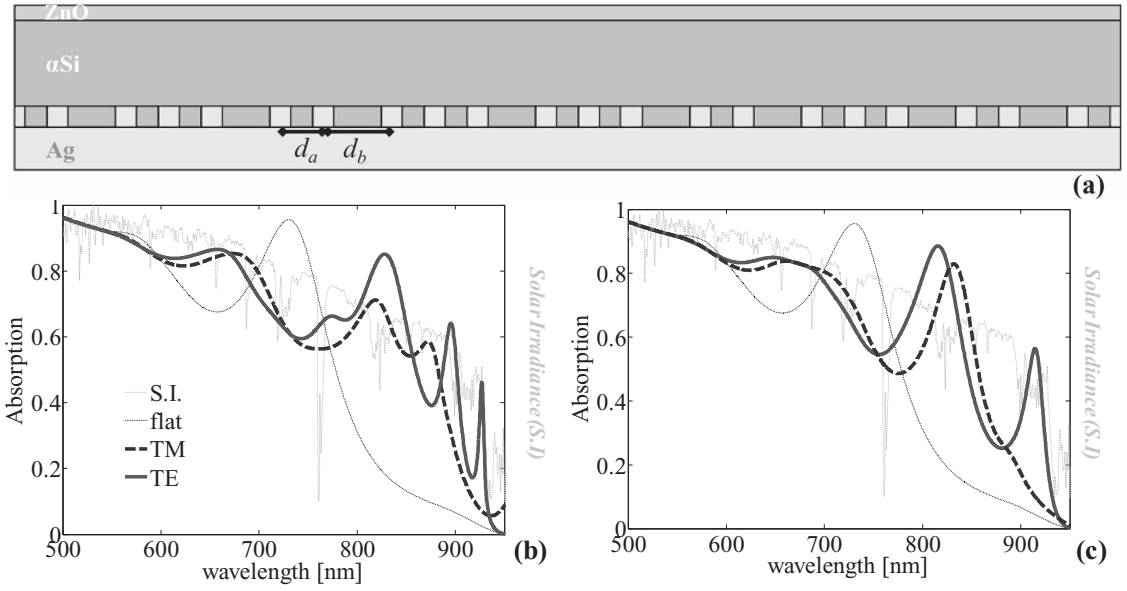


**Figure 8.** a) Schematic (supercell for numerical simulation) of the solar cell with a Fibonacci-like nanograting as backreflector. b) AM 1.5 solar spectrum; absorption spectra for the TE polarization (solid lines) and TM polarization (dashed lines) of the structure in (a); absorption spectrum of the solar cell with a silver mirror as backreflector (dotted lines). c) Same as (b), but with a periodic grating as backreflector.

small active regions (hundreds of square nanometers) leading to a significant reduction of the required amount of bound biomolecules in order to yield a given local refractive-index change. For much larger active areas (hundreds of square microns) as in our configuration and similar surface sensitivities, one accordingly needs the binding of a larger amount of biomolecules in order to experience the same local refractive-index change, with the consequent limitations in the detection limit. Nevertheless, the reported evidence paves the way to the development of novel cost-effective, large-area, high-throughput biological immunoassays with improved sensitivity with respect to real-world GR-based PC biosensors currently available on the market.[44,45]

## 4. Absorption Enhancement in Thin Film Solar Cells with Quasi-Periodic Backreflectors

The ability to engineer the plasmonic and photonic resonances (e.g., number and spectral locations) may provide new solutions in a variety of highly strategic fields, such as thin-film solar cells. In this context, it is well known that a serious limitation to the overall efficiency stems from the poor light absorption, especially at longer wavelengths of the solar spectrum, which is in turn attributable to the limited thickness of the semiconductor (active) region with respect to the absorption length of near infrared photons.[13] Accordingly, over the last few years, light-trapping techniques have been proposed in order to increase the optical thickness of the absorbing layer. A particularly promising approach relies on the use of metallic nanogratings on the back surface, which can couple the incoming radiation into both plasmonic (excited at the metal/semiconductor interface) and photonic modes (guided directly in the semiconductor layer).[13] In such configurations, the patterned metallic backreflector is capable of efficiently coupling the incoming light into photonic and plasmonic modes whose field distributions are mainly localized in the active region of the solar cell.[46] In this framework, QC backreflectors may be exploited to judiciously tailor the number and location of photonic/plasmonic modes within the near-infrared wavelength range, so as to enhance the overall performance.

As a representative example, we evaluate the performance of a 1D nanograting based on the generalized- Fibonacci deterministic aperiodic sequence (see also the Supporting Information).[34] The proposed solar-cell structure is shown in **Figure 8**a. It essentially consists of a 50 nm thick top layer of ZnO acting as a transparent electrode, a light-absorbing amorphous silicon middle layer (active region) with a thickness of 200 nm, and a silver nanograting which also serves as the bottom electrode. The grating is constituted of ridges of thickness 50 nm, placed according to the generalized-Fibonacci geometry with the scale-ratio parameter $\nu = d_b/d_a = \tau$ (where $d_a$ and $d_b = \nu d_a$ denote the two scales of the model, and $\tau = \left(1+\sqrt{5}\right)/2$ the Golden mean) and width $W = 0.3 d_{av}$, with $d_{av} = (d_a + \tau d_b)/(1+\tau) = 425$ nm denoting the average spacing. The grating grooves are filled with amorphous silicon.

The light absorption is calculated[46] as the flux of the Poynting vector (real part) through the surface of the amorphous-silicon layer (including the grooves) when the structure is illuminated by a normally incident plane wave. Similar considerations as for the previously studied (octagonal) structure hold, with the periodic approximant shown in Figure 8a (21-element supercell) simulated via COMSOL Multiphysics.[25,26] The ZnO refractive index was extracted directly from measurements (1.96 at $\lambda = 500$ nm, and 1.77 at $\lambda = 950$ nm).

Figure 8b shows the absorption spectra within the wavelength range 500–950 nm for both the transverse-electric (TE) and transverse-magnetic (TM) polarizations ($A_{TE}(\lambda)$ and

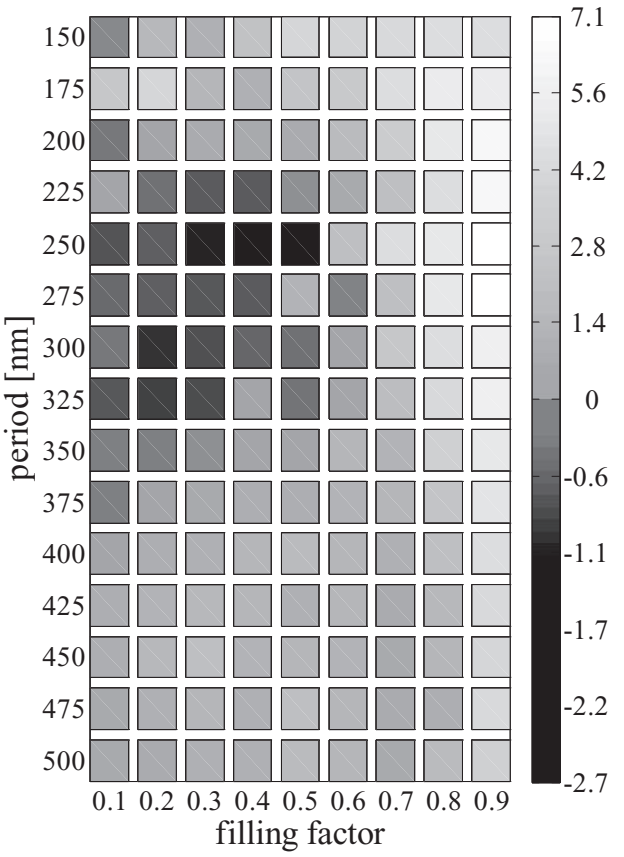


**Figure 9.** Total-absorption excess enhancement figure of merit $E'$ in (4), pertaining to a Fibonacci-like grating with respect to a periodic one, as function of the (average) period and filling factor.

$A_{TM}(\lambda)$, respectively), overlayed on the AM 1.5 normalized solar spectrum $S(\lambda)$.[46] Several absorption peaks can be observed, each of which may attributable to the excitation of i) cavity resonances due to the Fabry-Peròt effect, ii) guided photonic modes in the amorphous-silicon planar waveguide, or iii) plasmonic modes at the semiconductor-metal interface (only for the TM case).[46] A detailed discussion and classification of these three effects is beyond the scope of the present work. Also shown in Figure 8b is the absorption spectrum $A_{flat}(\lambda)$ of the same solar cell with a flat silver mirror in place of the grating. The total-absorption excess enhancement factor $E$ with respect to this reference configuration, defined as

$$E = 100\left(\frac{\eta_{Fibonacci}}{\eta_{flat}} - 1\right) \tag{1}$$

with

$$\eta_{Fibonacci} = \frac{1}{2}\left[\int A_{TE}(\lambda)S(\lambda)\,d\lambda + \int A_{TM}(\lambda)S(\lambda)\,d\lambda\right] \tag{2}$$

$$\eta_{flat} = \int A_{flat}(\lambda)S(\lambda)\,d\lambda \tag{3}$$

was found to be 14.7%. As a comparison, Figure 8c shows the absorption spectra pertaining to a periodic nanograting ($\nu = 1$, i.e., $d_a = d_b$) with same average spacing and filling factor. In this case, fewer absorption peaks (for both polarizations) can be observed, likely attributable to the lower number of photonic and plasmonic modes excited in the structure, resulting in a 2.2% lower enhancement factor.

In order to facilitate direct comparison between periodic and aperiodic nanogratings, as a figure of merit, we evaluated the total-absorption excess enhancement factor

$$E' = 100\left(\frac{\eta_{Fibonacci}}{\eta_{periodic}} - 1\right) \tag{4}$$

(with $\eta_{periodic}$ defined as in (3) but for a periodic grating) for different combinations of the average period (within the range 150–500 nm) and filling factor (within 10% to 90%), with results summarized as a grayscale plot in **Figure 9**. As it can be observed, for certain parameter combinations (dark pixels), the periodic grating may yield higher absorption, up to 2.7% in the figure of merit (4). However, though not fully optimized (the scale ratio $\nu = d_b/d_a$ being fixed), the Fibonacci grating turns out to attain higher absorption for most parameter combinations (light pixels), up to 7% in the figure of merit (4).

## 5. Conclusions

In conclusion, we have reported here the first evidence of out-of-plane resonances in hybrid metallo-dielectric QC nanostructures. Via measurements and full-wave numerical simulations on structures characterized by octagonal (Ammann-Beenker) geometry, we have observed the presence of sharp resonant dips in the reflectance spectrum, attributable to the excitation of plasmonic and photonic resonant modes, and verified the actual applicability of periodic-approximant-based computationally affordable design tools.

By comparison with a reference periodic (square) structure with same filling factor, the proposed QC structure exhibits a moderately richer resonant spectrum, which is attributable to the easier achievement of phase-matching conditions endowed by its denser Bragg spectrum. Moreover, the measured $Q$-factors, in the QC and periodic cases, turn out to be comparable and higher than those observed in periodic patterned fully metallic nanostructures.[28–31] We have also assessed the surface sensitivity with respect to nanosized deposition of SiO overlays (for response tuning/optimization), and $SiO_2$ overlays (with refractive index resembling that of biological molecules). The proposed metallo-dielectric QC nanostructures exhibit remarkably high surface sensitivity, namely, ~0.4 nm wavelength shift per nanometer of deposited $SiO_2$ overlay, with an enhancement of 50% with respect to the plasmonic resonances in the periodic counterpart. By acting on the extra degrees of freedom typical of QCs, there exist further margins of optimization for the surface sensitivity, and therefore concrete perspectives to outperform PC-based chemical and biological sensors based on periodic nanostructures currently available on the market.

Finally, we have shown that the resonance-engineering capabilities of QC nanostructures, in terms of tailoring the number and spectral positions of plasmonic and photonic resonances, may be effectively exploited in order to enhance the efficiency of thin film solar cells.

Overall, the results and examples illustrated here pave the way to the development of novel nanodevices, with possible applications to a variety of highly strategic fields, ranging from chemical and biological sensing to energy harvesting.

## 6. Experimental Section

*Structure Fabrication*: The nanometer-size patterns of the hybrid metallo-dielectric nanostructure considered in this study (and schematically represented in Figure 1a) were defined in an electron-beam positive resist by standard electron beam lithography (EBL). A 30 nm film of aluminum was first deposited on a sapphire substrate by direct-current magnetron sputtering in an ultra-high vacuum system at a base pressure of $8 \times 10^{-8}$ Torr. The sample was then spin-coated with ~ 370 nm of electron-beam positive resist (ZEP 520A, Zeon Chemicals) and baked on a hot plate for 2 min at 180 °C. Subsequently, a 400 × 400 $\mu m^2$ matrix of circular holes (placed at the tiling vertices) was patterned on the same substrate by using a Raith 150 EBL system with a voltage of 20 kV and a dose of 55 $\mu C/cm^2$. In this process, the metallic film also acts as a charge dissipation layer to avoid deflection of the electron-beam during the writing process. After the electron-beam exposure, the sample was developed in a ZED N50 solution (Zeon Chemicals) for 45 s, and subsequently rinsed in isopropanol.

*Measurement Setup*: For the out-of-plane reflectance measurements, we utilized a broad-band white light source directly coupled into a standard fiber-based reflection probe acting simultaneously as light launcher and collector. The reflection probe illuminates the entire patterned area via an optical fiber bundle with six outside fibers in ring-shaped configuration. The light reflected by the sample (placed on a motorized XYZ positioning stage enabling a 10 μm absolute on-axis accuracy) is collected by a central fiber (with a collection spot diameter ≈350 μm) directly connected to an optical spectrum analyzer operating with a resolution of 0.4 nm. As a tradeoff between the fulfilling of paraxial (normal incidence) conditions and an adequate signal-to-noise ratio, we selected a distance of 7 mm between the sample and the reflection probe. The measured reflectance spectra were finally normalized with respect the (known) reference response of an aluminum mirror.

## Supporting Information

Supporting Information is available from the Wiley Online Library or from the author.

## Acknowledgements

The kind assistance of Prof. Luca Palmieri (University of Padova, Italy) in the numerical simulations is gratefully acknowledged.

Received: January 23, 2012
Revised: May 8, 2012
Published online: June 13, 2012

[1] S. A. Maier, in *Plasmonics: Fundamentals and applications*; Springer, Berlin **2007**.
[2] *Handbook of surface plasmon resonance*; (Eds: R. B. M. Schasfoort, A. J. Tudos), RSC Publishing, Cambridge, UK **2008**.
[3] E. Hutter, J. Fendler, *Adv. Mater.* **2004**, *16*, 1685.
[4] J. D. Joannopoulos, S. G. Johnson, R. D. Meade, J. N. Winn, *Photonic crystals: Molding the flow of light, second edition*, Princeton University Press, Princeton NJ **2008**.
[5] S. Fan, J. D. Joannopoulos, *Phys. Rev. B* **2002**, *65*, 235112.
[6] X. Li, D. Han, F. Wu, C. Xu, X. Liu, J. Zi, *J. Phys.: Condens. Matter* **2008**, *20*, 485001.
[7] X. Yu, L. Shi, D. Han, J. Zi, P. V. Braun, *Adv. Funct. Mater.* **2010**, *20*, 1910.
[8] M. López-García, J. F. Galisteo-López, A. Blanco, J. Sánchez-Marcos, C. López, A. García-Martín, *Small* **2010**, *6*, 757.
[9] M. López-García, J. F. Galisteo-López, A. Blanco, C. López, A. García-Martín, *Adv. Funct. Mater.* **2010**, *20*, 4338.
[10] X. Zhu, L. Shi, X. Liu, J. Zi, J. Wang, *Nano Res.* **2010**, *3*, 807.
[11] L. Shi, X. Liu, H. Yina, J. Zi, *Phys. Lett. A* **2010**, *374*, 1059.
[12] S. G. Romanov, A. V. Korovin, A. Regensburger, U. Peschel, *Adv. Mater.* **2011**, *22–23*, 2515.
[13] H. A. Atwater, A. Polman, *Nat. Mater.* **2010**, *9*, 205.
[14] F. Przybilla, C. Genet, T. W. Ebbesen, *Appl. Phys. Lett.* **2006**, *89*, 121115.
[15] T. Matsui, A. Agrawal, A. Nahata, Z. V. Vardeny, *Nature* **2007**, *446*, 517.
[16] A. Gopinath, S. V. Boriskina, N.-N. Feng, B. M. Reinhard, L. Dal Negro, *Nano Lett.* **2008**, *8*, 2423.
[17] A. Gopinath, S. V. Boriskina, W. R. Premasiri, L. Ziegler, B. M. Reinhard, L. Dal Negro, *Nano Lett.* **2009**, *9*, 3922.
[18] S. V. Boriskina, S. Y. K. Lee, J. J. Amsden, F. G. Omenetto, L. Dal Negro, *Opt. Express* **2010**, *18*, 14568.
[19] A. Ricciardi, M. Pisco, A. Cutolo, A. Cusano, L. O'Faolain, T. F. Krauss, G. Castaldi, V. Galdi, *Phys. Rev. B* **2011**, *84*, 085135.
[20] D. Shechtman, I. Blech, D. Gratias, J. W. Cahn, *Phys. Rev. Lett.* **1984**, *53*, 1951.
[21] D. Levine, P. J. Steinhardt, *Phys. Rev. Lett.* **1984**, *53*, 2477.
[22] M. Senechal, *Quasicrystals and geometry*; Cambridge University Press, Cambridge, UK **1995**.
[23] S. Fischer, A. Exner, K. Zielske, J. Perlich, S. Deloudi, W. Steurer, P. Lindner, S. Förster, *Proc. Natl. Acad. Sci. USA* **2011**, *108*, 1810.
[24] U. Grimm, M. Schreiber, in *Quasicrystals: an introduction to structure, physical properties, and applications*, (Eds: J.-B. Suck, M. Schreiber, P. Häussler), Springer, Berlin **2002**.
[25] Comsol Multiphysics, http://www.comsol.com (accessed November 2011)
[26] RefractiveIndex.Info, http://refractiveindex.info (accessed November 2011).
[27] G. Nemova, R. Kashyap, *Opt. Commun.* **2007**, *275*, 76.
[28] T. W. Ebbesen, H. J. Lezec, H. F. Ghaemi, T. Thio, P. A. Wolff, *Nature* **1998**, *391*, 667.
[29] J. Aizpurua, P. Hanarp, D. S. Sutherland, M. Käll, G. W. Bryant, F. J. García de Abajo, *Phys. Rev. Lett.* **2003**, *90*, 4.
[30] A. D. McFarland, R. P. Van Duyne, *Nano Lett.* **2003**, *3*, 1057.
[31] J. Henzie, M. H. Lee, T. W. Odom, *Nat. Nanotechnol.* **2007**, *2*, 549.
[32] S. Peng, G. M. Morris, *J. Opt. Soc. Am. A* **1996**, *13*, 993.
[33] R. E. Collin, *Field theory of guided waves*, *2nd Ed*. IEEE Press, Piscataway, NJ **1991**.
[34] P. Buczek, L. Sadun, J. Wolny, *Acta Phys. Polon. B* **2005**, *36*, 919.
[35] A. Cusano, A. Iadicicco, P. Pilla, L. Contessa, S. Campopiano, A. Cutolo, M. Giordano, *Opt. Lett.* **2005**, *30*, 2536.
[36] A. Tsargorodskaya, A. V. Nabok, A. K. Ray, *Nanotechnology* **2004**, *15*, 703.
[37] D. Piscevic, W. Knoll, M. J. Tarlov, *Supramol. Sci.* **1995**, *2*, 99.
[38] M. Pisco, A. Ricciardi, I. Gallina, G. Castaldi, S. Campopiano, A. Cutolo, A. Cusano, V. Galdi, *Opt. Express* **2010**, *18*, 17280.
[39] T. Vo-Dinh, *IEEE J. Sel. Top. Quantum Electron.* **2008**, *14*, 1989.

[40] F. Vollmera, S. Arnold, D. Keng, *Proc. Natl. Acad. Sci. USA* **2008**, *105*, 20701.
[41] F. De Angelis, M. Patrini, G. Das, I. Maksymov, M. Galli, L. Businaro, L. C. Andreani, E. Di Fabrizio, *Nano Lett.* **2008**, *8*, 2321.
[42] T. Lu, H. Lee, Tong Chen, S. Herchak, J.-H. Kim, S. E. Fraser, R. C. Flagan, K. Vahala, *Proc. Natl. Acad. Sci. USA* **2011**, *108*, 5976.
[43] J. L. Dominguez-Juarez, G. Kozyreff, J. Martorell, *Nat. Commun.* **2011**, *2*, 254.
[44] N. Ganesh, W. Zhang, P. C. Mathias, E. Chow, J. A. N. T. Sooares, V. Malyarchuk, A. D. Smith, B. T. Cunningham, *Nat. Nanotechnol.* **2007**, *2*, 515.
[45] B. T. Cunningham, I. D. Block, L. Chan, N. Ganesh, M. Lu, P. C. Mathias, in *Selected topics in photonic crystals and metamaterials* (Eds: A. Andreone, A. Cusano, A. Cutolo, V. Galdi), World Scientific, Singapore **2011**, Ch. 12.
[46] W. Wang, S. Wu, K. Reinhardt, Y. Lu, S. Chen, *Nano Lett.* **2010**, *10*, 2012.